RSC Advances

ROYAL SOCIETY OF CHEMISTRY

www.rsc.org/advances

Journal Name

RSCPublishing

ARTICLE

Effect of dye end groups in non-fullerene fluorene- and carbazole-based small molecule acceptors on photovoltaic performance

Cite this: DOI: 10.1039/x0xx00000x

Received 00th January 2012,
Accepted 00th January 2012

DOI: 10.1039/x0xx00000x

www.rsc.org/

Yujeong Kim,[a] Chang Eun Song,[b] Sang-Jin Moon,[b] Eunhee Lim*[a]

Six small molecules with three different dye units, ethyl cyanoacetate (ECA), 1,3-indandione (IN), and 3-ethylrhodanine (RH), attached to both ends of thiophene-flanked carbazole (Cz) or fluorene (Flu) cores were synthesized and used as acceptors in organic photovoltaic cells (OPVs). Their optical and electrochemical, and consequent photovoltaic parameters varied mainly according to the dye units. The OPV cells were fabricated with the configuration ITO/PEDOT:PSS/poly(3-hexylthiophene):small molecule/LiF/Al and all devices except for **Cz-IN** showed photovoltaic performances with power conversion efficiencies (PCEs) in the range of 1.03–3.08% and open-circuit voltages as high as 1.03 V. Among them, the **ECA** and **RH series** had relatively high open-circuit voltages values because of their high-lying lowest unoccupied molecular orbital energy levels. Devices based on **Flu-IN** and the **RH series** showed high short-circuit currents (J_{SC}) because of the strong molecular aggregation, as evidenced by red-shifted UV absorption from solution to film. The adequate molecular aggregation in **Flu-IN** and **RH** films enhanced electron transport between the molecules, resulting in devices with high J_{SC} and PCE values. This work demonstrates that the introduction of dye end units onto carbazole- and fluorene-based small molecules provides good candidates for non-fullerene acceptors.

1. Introduction

Organic photovoltaic cells (OPVs) have drawn significant attention as a promising renewable energy technology.[1] In recent years, solution-processed bulk-heterojunction (BHJ) solar cells have been developed with advantages such as low-cost manufacturing and flexible device fabrication.[2] The donor and acceptor materials used in the active layer have been actively developed to achieve high-performance BHJ solar cells. With the rapid progress in the development of donor materials, power conversion efficiencies (PCE) of 10.6%[3] and 10.1%[4] have been reported in tandem devices using polymeric and small molecular donors, respectively, in combination with fullerene derivatives as acceptors.

Compared to the advancement of donor materials, the development of acceptors has progressed slowly and most OPV cells have been fabricated using fullerene derivatives such as [6,6]-phenyl-C_{61} butyric acid methylester ($PC_{61}BM$).[5] Fullerene derivatives are widely used because of their good electron mobility and interactions with donor materials;[6] however, they also have some drawbacks such as difficult synthesis and purification and weak absorption in the visible region.[7] The importance of the development of new non-fullerene acceptors has been recently emphasized by virtue of their easy synthesis, adjustable frontier orbital energy levels and high absorbance in the solar spectrum.[8] The electron withdrawing backbones of the acceptors include perylene bisimide (PBI),[9-11] naphthalene diimide,[12] and benzothiadiazole.[13] Up to now, devices using polymeric non-fullerene acceptors have reached efficiencies of up to 6.4%,[14] confirming the possibility of substituting fullerene acceptors such as $PC_{61}BM$ with non-fullerene acceptors. Non-fullerene small molecule acceptors have also been reported to exhibit efficiencies as high as polymeric acceptors with a maximum PCE of 5.9% observed using a bay-linked di-PBI acceptor.[11] These small molecules have advantages such as easier energy level control by versatile functional-group substitution and less batch-to-batch variation. Recently, much improvement in the performance of non-fullerene acceptor-based devices has been achieved by combining various donors instead of representative donors such as poly(3-hexylthiophene) (P3HT).[10-11,15]

Furthermore, dye units such as ethyl cyanoacetate (ECA),[16] 3-ethylrhodanine (RH),[17,18] and 1,3-indandione (IN),[19-20] have been introduced as terminal electron-withdrawing groups onto the electron-rich backbone of oligothiophenes and/or benzo[1,2-b:4,5-b']dithiophene (BDT) to make high performance low band-gap small molecule donor materials. For example, a BDT-based small molecule donor (DR3TSBDT) with RH dye end units exhibited a high PCE of 9.95%,[18] which was the best PCE observed using a small molecule donor in single-junction OPVs. Very recently, our group introduced RH dye end units into the carbazole and fluorene backbones and used them as electron acceptors combined with a P3HT donor.[21] A high PCE of up to 3.08% was obtained in combination with a high V_{OC} of over 1 V. Similar researches

were also reported by S. E. Watkins and I. McCulloch groups, observing PCEs of 2.43%[22] and 4.11%,[23] respectively, from P3HT and a fluorene-dye-based acceptor. From this, we concluded that the introduction of dye units onto both ends of the small molecules could be a good strategy for developing new non-fullerene acceptors as well as small molecular donors with high OPV device performance.

Herein, we introduced three different dye end units, ECA, IN and RH, onto carbazole and fluorene backbones and compared their physical properties. OPV cells were then fabricated using these molecules as acceptors and P3HT as the donor. Device performance was affected by the electron-withdrawing and packing abilities of the dye units. The thermal, optical and electrochemical properties and film morphologies of the small molecules were systematically investigated by differential scanning calorimetry (DSC), thermogravimetric analysis (TGA), UV absorption spectroscopy, cyclic voltammetry (CV), and atomic force microscopy (AFM).

2. Results and discussion

2.1 Synthesis and physical properties

Six small molecules were synthesized by introducing electron-deficient dyes, ECA, RH, and IN, onto both ends of electron-rich thiophene-flanked carbazole (Cz) or fluorene (Flu) cores for use as acceptors in BHJ solar cells. Initially, 2,7-diboronic esters of carbazole and fluorene were reacted with 2-bromo-5-formylthiophene using the palladium-catalyzed Suzuki coupling reaction to synthesize two diformyl compounds (Cz-T-CHO and Flu-T-CHO).[21] Subsequently, the six small molecules were synthesized by Knoevenagel condensation of the diformyl compounds and dyes resulting in good yields (67–86%). All the small molecules displayed good solubility in common organic solvents such as chloroform, chlorobenzene, and *o*-dichlorobenzene (*o*-DCB). Their chemical structures were characterized by ^{1}H NMR, ^{13}C NMR (Fig. S1–S8†), and elemental analysis (EA) and are shown alongside their synthetic routes in Scheme 1. The thermal characteristics of the small molecules were investigated using DSC and TGA (Fig. 1). All the small molecules were sufficiently thermally stable for use in OPV applications showing weight losses of 5% up to 360 °C. In DSC, the **IN series** showed higher melting points than the **ECA** and **RH series**.

Fig. 2 shows the UV-visible absorption spectra of the small molecules in solution and thin solid films prepared from *o*-DCB. The absorption spectra of the small molecules depended on their dye end unit, and the **ECA**, **RH**, and **IN series** solutions had absorption maxima (λ_{max}) at around 460, 501, and 518 nm, respectively. As films, remarkable red-shifts were observed in the absorption spectra of the **RH** and **IN** films ($\Delta\lambda$ = 26–67 nm) compared to the solutions, indicative of strong molecular aggregation between molecules, whereas the absorption profiles of the **ECA** films were slightly broadened and much less red-shifted ($\Delta\lambda$ = 0–8 nm). Particularly, the **Cz-IN** film exhibited vibronically well-structured absorption bands with λ_{max} at 577 nm. The optical band gaps (E_g^{opt}) of the small molecules were calculated from their onset of absorption (E_g^{opt}= 1240/λ_{onset} eV) and were in the range of 2.00–2.33 eV (Table 1). The Cz-based small molecules had a slightly narrower E_g^{opt} than the corresponding Flu-based molecules. More importantly, E_g^{opt} gradually decreased from the **ECA** via **RH** to **IN series** and the large red shifts ($\Delta\lambda$) observed in the **IN** and **RH** films resulted in relatively low E_g^{opt} values that were as low as 2.00 eV.

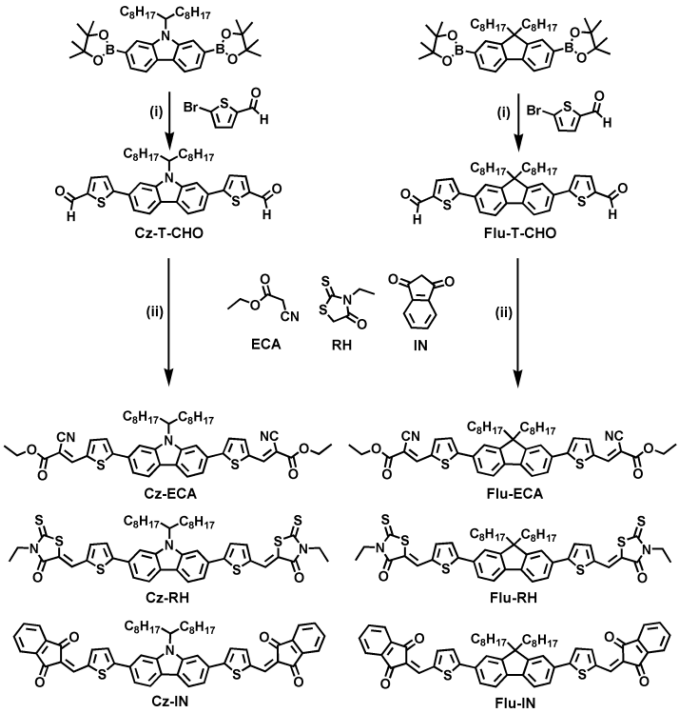

Scheme 1 Synthetic schemes and chemical structures of the small molecules: (i) $Pd(PPh_3)_4$, DME, Na_2CO_3 (*aq*, 1 M), 80 °C, N_2 for 4 h; (ii) Knoevenagel condensation.

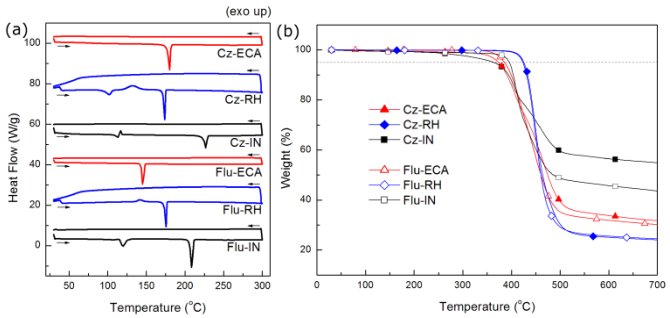

Fig. 1 (a) DSC and (b) TGA curves of the small molecules.

The electrochemical properties of the small molecules were characterized by CV measurements (Fig. 2(c)). The highest occupied molecular orbital (HOMO) and lowest unoccupied molecular orbital (LUMO) energy levels were calculated using the equation $E_{HOMO} = -(E_{onset,ox} - E_{1/2,ferrocene} + 4.8)$ eV and $E_{LUMO} = -(E_{onset,red} - E_{1/2,ferrocene} + 4.8)$ eV, where $E_{onset,ox}$ and $E_{onset,red}$ are the onset potentials of oxidation and reduction, respectively, assuming that the energy level of ferrocene (Fc) is 4.8 eV below the vacuum level.[24] The electrochemical energy band gaps (E_g^{CV}) were estimated from the onset potentials of the oxidation and reduction processes ($E_g^{CV} = E_{HOMO} - E_{LUMO}$) and are listed in Table 1. Compared to the **ECA series** (e.g., 2.15 eV for **Cz-ECA**), the **RH** and **IN series** had relatively small E_g^{CV} values (e.g., 2.03 eV for **Cz-RH** and 1.99 eV for **Cz-IN**), which were in agreement with the trend observed in E_g^{opt}. The LUMO energy levels (E_{LUMO}^{opt}), shown in Fig. 2(d) and Table 1, were estimated using HOMO energy levels and the optical E_g^{opt} ($E_{LUMO}^{opt} = E_{HOMO} + E_g^{opt}$). While the E_g^{opt} values of the **ECA series** were larger than the E_g^{CV} values (e.g., $\Delta E_g = E_g^{opt} - E_g^{CV}$ = 0.11 eV), the **RH** and **IN series** had similar E_g^{opt} and E_g^{CV} values (e.g., $\Delta E_g = \pm 0.05$). In other words,

Table 1 Physical properties of the small molecules

Acceptor	T_m (℃)[a]	T_{5d} (℃)[b]	λ_{max} (nm) soln	λ_{max} (nm) Film	$\Delta\lambda$ (nm)[c]	E_g^{opt} (eV, UV/nm)[d]	HOMO (eV)	$LUMO^{opt}$ (eV)[e]	E_g^{CV} (eV)[f]	$LUMO^{CV}$ (eV)	ΔE_g (eV)[g]
Cz-ECA	179	374	465	473	8	2.26 (549)	–5.63	–3.37	2.15	–3.48	0.11
Cz-RH	174	426	501	568	67	2.05 (605)	–5.53	–3.48	2.03	–3.50	0.02
Cz-IN	227	364	519	577	58	2.00 (620)	–5.57	–3.57	1.99	–3.58	0.01
Flu-ECA	145	386	459	459	0	2.33 (532)	–5.70	–3.37	2.22	–3.48	0.11
Flu-RH	175	424	501	550	49	2.10 (591)	–5.58	–3.48	2.05	–3.53	0.05
Flu-IN	208	396	518	544	26	2.07 (599)	–5.70	–3.63	2.12	–3.58	-0.05

[a] T_m was the melting temperature. [b] T_{5d} was the decomposition temperature at which a weight loss of 5% was observed. [c] $\Delta\lambda = \lambda_{max}$ (film) – λ_{max} (soln). [d] E_g^{opt} was calculated from the onset of absorption (value in parenthesis) of the UV-vis spectrum of the film ($E_g^{opt} = 1240/\lambda_{onset}$ eV). [e] E_{LUMO}^{opt} was estimated using the HOMO level and E_g^{opt} ($E_{LUMO}^{opt} = E_{HOMO} + E_g^{opt}$). [f] E_g^{CV} was estimated from the onset potentials of the oxidation and reduction processes ($E_g^{CV} = E_{HOMO} - E_{LUMO}^{CV}$). [g] ΔE_g is the difference between E_g^{opt} and E_g^{CV} ($\Delta E_g = Eg^{opt} - E_g^{CV}$).

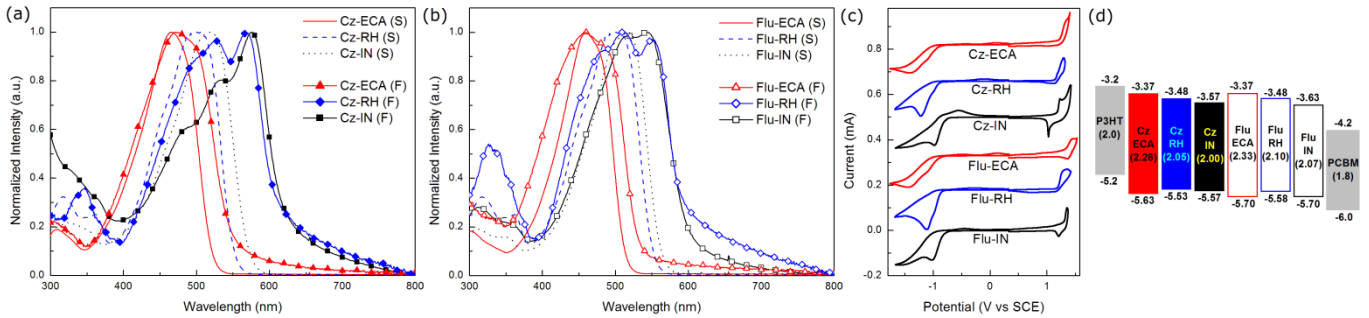

Fig. 2 UV-vis absorption spectra of (a) Cz- and (b) Flu-based small molecules in solution (S) and films (F), (c) CV curves, and (d) the energy diagram of the small molecules together with P3HT and $PC_{61}BM$ (E_g^{opt} are shown in parenthesis).

the strong molecular aggregation in the **RH** and **IN** films led to remarkable red-shifts in film absorption and decreases in E_g^{opt} compared to the **ECA** films.

More importantly, all six molecules showed relatively high-lying LUMO energy levels in the range of –3.37 eV to –3.63 eV (Table 1), compared to $PC_{61}BM$ (–4.20 eV), which could be responsible for their increased open-circuit voltage (V_{OC}) in OPVs.[25] Among the six molecules, the **ECA** and **RH series** had the higher LUMO energy levels of –3.37 and –3.48 eV, respectively, compared to those of the **IN series**. It is worth noting that, despite the high-lying LUMO levels of the acceptors, a sufficient offset exists between the LUMO energy levels of P3HT (–3.2 eV) and the acceptors, for efficient charge generation.[26] In addition, the Cz- and Flu-based analogs with the same dye units showed similar LUMO energy levels. For example, **Cz-ECA** and **Flu-ECA** had the same LUMO energy levels (–3.37 eV). It is well known that the LUMO energy levels of the molecules are mainly determined by their electron-withdrawing moieties, whereas the HOMO energy levels are decided by their electron-donating moieties.[27] The energy diagram of the small molecules is shown in Fig. 2(d) together with the energy levels of P3HT and $PC_{61}BM$ for comparison.[28]

2.2 Photovoltaic Performances

Fig. 3 shows the current-density *versus* voltage (*J*–*V*) curves and external quantum efficiency (EQE) curves measured in air under white light AM 1.5 illumination (100 mW/cm^2), and selected photovoltaic properties of the films are summarized in Table 2. OPV devices were fabricated with the configuration ITO/PEDOT:PSS/P3HT:small molecules/LiF/Al. The D:A blend ratios and annealing temperatures (T_a) were optimized (Table S1–S2 and Fig. S9†). All devices except for **Cz-IN** showed photovoltaic characteristics with PCE values over 1%. Among them, the best performance was achieved for acceptors with RH dye end groups. The optimized P3HT:**Flu-RH** device exhibited a PCE of 3.08% with a high V_{OC} of 1.03 V and a moderate J_{SC} and fill factor, which was comparable to the PCE of P3HT:$PC_{61}BM$ (3.34%) fabricated under the same conditions. In addition, the small molecule:$PC_{71}BM$ devices showed no photovoltaic characteristics (Fig. S10 and Table S3†).

OPV cells based on all the new Cz- and Flu-based acceptors exhibited high V_{OC} values in the range of 0.92–1.03 V, except for **Cz-IN**. These V_{OC} values are higher than P3HT:$PC_{61}BM$ (0.60 V) and can be easily explained by the high-lying LUMO energy level (Fig. 2(d)) of the acceptors. The relatively higher V_{OC} values up to 1.03 V for **ECA** and **RH series** also came from the relatively high-lying LUMO energy levels, as stated above.

In the **RH** and **ECA series**, the Flu-based small molecules showed a higher J_{SC} than their Cz-based analogs. For example, Flu-RH showed a higher J_{SC} (5.70 mA/cm^2) than **Cz-RH** (4.69 mA/cm^2) and **Flu-ECA** also showed a higher J_{SC} (2.82 mA/cm^2) than **Cz-ECA** (2.34 mA/cm^2). Such a trend has been explained in our previous report on RH-based small molecules, in which P3HT:**Flu-RH** film had a higher photoluminescence quenching efficiency than P3HT:**Cz-RH**, showing good charge separation between P3HT and the acceptor.[21] J_{SC} values also varied with the dye end groups and increased from **ECA** via **IN** to **RH**, with the exception of **Cz-IN**. The relatively high J_{SC} of the **RH** and **IN** series (except for **Cz-IN**) can be explained by the strong molecular aggregation observed by their remarkably red-shifted film absorption and the consequent increase in electron transport between acceptor molecules. Despite the high V_{OC} values of over 1.00 V, the PCEs of the **ECA series** are lower than those of the **Flu-IN** and **RH series** owing to their

relatively poor molecular stacking. The higher J_{SC} values of the **Flu-IN** and **RH series** are well-matched with their higher EQE intensities, as shown in Fig. 3. Maximum EQEs of around 40% were achieved in the devices made from **Flu-RH** and **Cz-RH**. **Flu-IN** and the **ECA series** also had good EQE responses with maximum intensities over 25%; however, the **ECA series** exhibited relatively low EQE responses for wavelengths over 500 nm, which was probably related to the blue-shifted absorption of the **ECA** films (Fig. 2).

Charge-carrier mobilities in blend films were measured using the space-charge limited current (SCLC) method. Hole- and electron-only devices were fabricated with the structures of ITO/PEDOT:PSS/P3HT:small molecule/Au and ITO/ZnO/P3HT:small molecule/Ca/Al, respectively. Fig. 4 shows the *J*–*V* curves of the P3HT:acceptor films for hole-only and electron-only devices together with a comparison between mobilities and J_{SC} values. The trends for the electron and hole mobilities are very consistent to the trend observed for the J_{SC} values of OPVs (Fig. 4(c)). RH-based acceptors with higher J_{SC} values exhibited relatively high electron and hole mobilities in both the **Flu-** and **Cz series**. **Flu-IN** also had slightly higher electron mobility than that of **Flu-ECA**; **Cz-IN** showed no hole or electron mobility. The charge mobility values are summarized in Table 2.

Table 2 Photovoltaic properties of BHJ solar cells[a]

Acceptor	D:A ratio	T_a (℃)[b]	V_{OC} (V)	J_{SC} (mA/cm^2)	FF (%)	PCE (%)	μ_h[d] (cm^2/Vs)	μ_e[e] (cm^2/Vs)
Cz-ECA	1.0:1.5	100	1.00 (0.98±0.02)	2.34 (2.21±0.14)	44 (42±1)	1.03 (0.98±0.07)	6.38×10^{-4}	3.24×10^{-4}
Cz-RH[c]	1.0:1.5	100	1.03 (1.00±0.01)	4.69 (4.44±0.17)	53 (52±1)	2.56 (2.44±0.12)	7.99×10^{-4}	3.94×10^{-4}
Cz-IN	1.0:1.5	100	0.61 (0.54±0.12)	0.13 (0.11±0.10)	26 (26±1)	0.02 (0.02±0.00)	-	-
Flu-ECA	1.0:1.0	100	1.03 (0.99±0.01)	2.82 (2.68±0.14)	44 (43±1)	1.26 (1.15±0.07)	6.67×10^{-4}	3.59×10^{-4}
Flu-RH[c]	1.0:1.5	100	1.03 (1.02±0.12)	5.70 (5.55±0.24)	52 (51±1)	3.08 (3.00±0.07)	8.54×10^{-4}	4.60×10^{-4}
Flu-IN	1.0:1.0	80	0.92 (0.90±0.02)	3.40 (3.31±0.08)	42 (40±1)	1.32 (1.21±0.11)	7.05×10^{-4}	3.81×10^{-4}

[a] Selected data for the optimized fabrication conditions with the average PCE and standard deviation based on more than 5 devices in parenthesis (PCE_{avg} ± std dev). [b] The films were annealed at T_a for 10 min. [c] Data taken from ref. 35. [d] The hole-only devices with structure of ITO/PEDOT:PSS/P3HT:acceptor/Au. [e] The electron-only devices with structure of ITO/ZnO/P3HT:acceptor /Ca/Al.

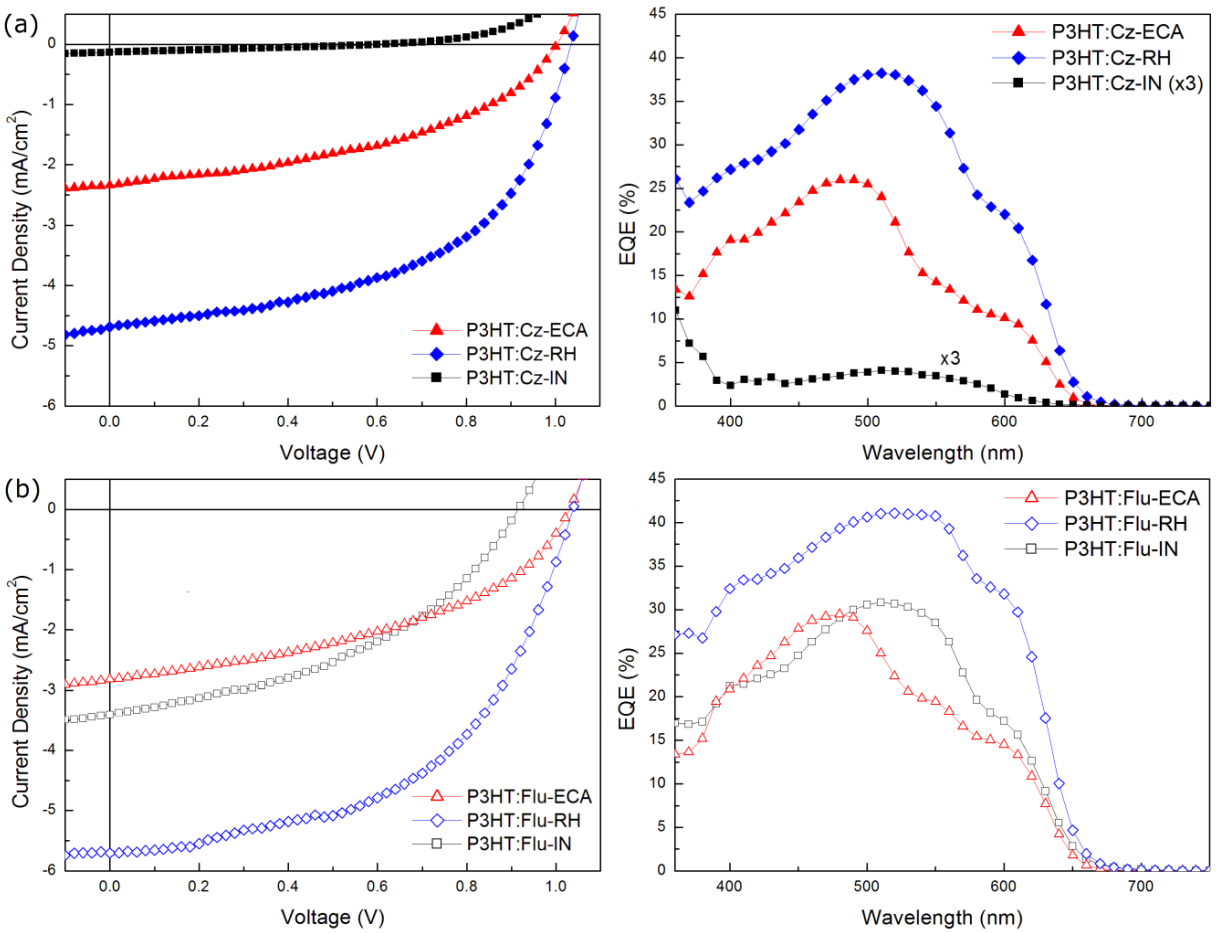

Fig. 3 *J*–*V* (left) and EQE (right) curves of (a) Cz- and (b) Flu-based small molecules.

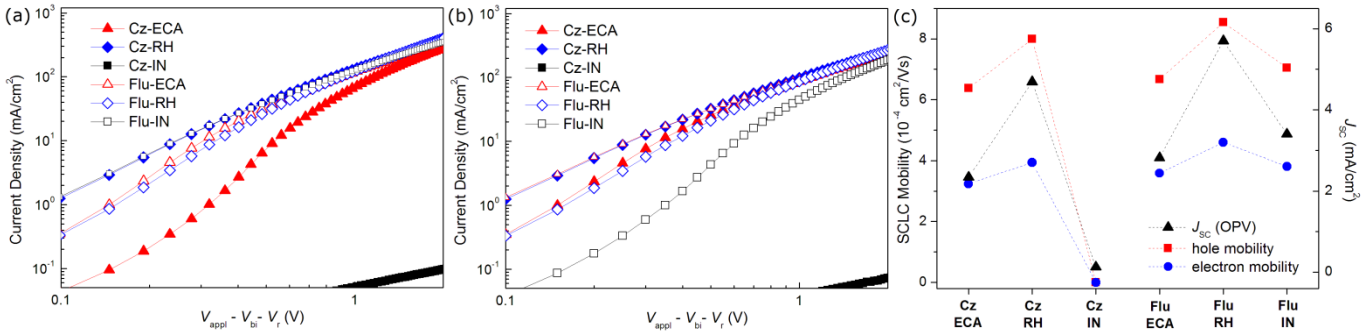

Fig. 4 Measured SCLC *J*–*V* characteristics of P3HT:acceptor devices for (a) hole- and (b) electron-only devices together with a comparison between mobilities and J_{SC} values (c).

Despite its remarkably red-shifted absorption and high-lying LUMO energy level that is similar to **Flu-IN**, the device fabricated from **Cz-IN** showed a very low performance (0.02%) with a marginal J_{SC} (0.13 mA/cm^2). This can be explained in terms of film morphology. AFM was performed to investigate the morphology of the active layers prepared with blend ratios optimized for OPV devices. The height and phase AFM images for the blend films are shown in Fig. 5 and Fig. S11†, respectively. Except for P3HT:**Cz-IN**, all blend films composed of P3HT and acceptor were very homogeneous with root-mean-square (rms) roughness values of 3.0–3.4 nm, similar to that of the P3HT:$PC_{61}BM$ film (rms = 2.9 nm). The nano-sized fibrillar crystallites were well dispersed throughout all regions and corresponded to crystalline P3HT nanofibers indicating the presence of large interfacial areas between the donor and acceptor.[29] In contrast, the P3HT:**Cz-IN** blend film had large rod-shaped grains, resulting in a very rough morphology (rms = 11.9 nm). These distinguishing features were caused by the exceptionally strong molecular aggregation of **Cz-IN** molecules, as supported by their red-shifted UV absorption with enhanced vibronic absorption. Carrier transport in the P3HT:**Cz-IN** film may decrease at these large grain boundaries resulting in a relatively low J_{SC} in OPVs. The high packing ability of the IN-based small molecules was previously reported by Y. Chen's group.[20] In their work, the efficient packing of the IN-containing oligothiophene (DIN7T) donor resulted in a higher performance (4.71 %) compared to similar oligothiophenes with poor stacking in OPVs. Generally, good molecular aggregation is advantageous for high OPV performance because it can provide increased charge transport between molecular backbones. In our systems, the **IN** and **RH series** had relatively higher molecular aggregation than the **ECA series**, which agreed well with the higher J_{SC} of **Flu-IN** and the **RH series** compared to the **ECA series**. However, the much stronger aggregation observed for **Cz-IN** resulted in large rod-shaped **Cz-IN** domains, which diminished good intermixing of donor and acceptor molecules. Similar decreases in photovoltaic properties were observed in the previous reports on oligothiophenes, in which the unfavorable morphology of large domains resulted in decreased charge transport at grain boundaries.[30] Optimized molecular aggregation should be guaranteed to achieve sufficient charge (in this case, electron) transport between molecules; however excessively strong aggregation could reduce charge transport. Therefore, control over the degree of molecular aggregation is important in gaining optimized film morphology.

In this work, we succeeded in easily controlling the packing ability of acceptors by changing their dye end groups and the relationship between their molecular structures and physical properties was systematically investigated. Further improvement in device performance could be obtained by molecular engineering such as modifying the thiophene bridge or alkyl chains, together with device optimization by using other donor materials instead of P3HT and alternative device architectures.

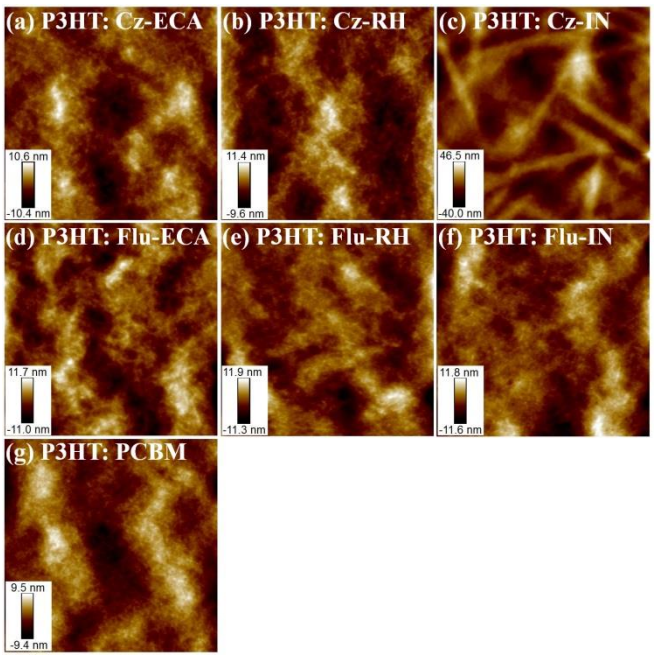

Fig. 5 AFM images (2 x 2 μm) of (a) P3HT:**Cz-ECA**, (b) P3HT:**Cz-RH**, (c) P3HT:**Cz-IN**, (d) P3HT:**Flu-ECA**, (e) P3HT:Flu-**RH**, (f) P3HT:**Flu-IN**, and (g) P3HT:$PC_{61}BM$ films.

3. Conclusions

A series of small molecules was synthesized by introducing various dye units, ECA, RH, and IN, onto carbazole or fluorene backbones for use as acceptors in OPVs. All devices, except for that based on **Cz-IN**, showed good photovoltaic performances with PCEs of up to 3.08% and characteristic high V_{OC} values of up to 1.03 V. The electron-withdrawing and packing abilities of the molecules that varied according to the dye end groups affected the physical properties and photovoltaic parameters of the acceptors. The **RH** and **ECA series** had relatively high V_{OC} values because of their high-lying LUMO energy levels. Compared to the **ECA series**,

relatively high J_{SC} values were achieved for the **Flu-IN** and **RH series** owing to good molecular aggregation in these films; however, the excessively strong aggregation observed in **Cz-IN** resulted in films with poor morphology that contained large rod-shaped grains, and exhibited very low performance. The adequate molecular aggregation in the **Flu-IN** and **RH** films enhanced electron transport between the molecules, resulting in devices with high J_{SC}. In this work, we easily controlled the degree of molecular aggregation by introducing different dye end groups and successfully demonstrated that dye-functionalized carbazole and fluorene are good candidates for use as non-fullerene electron acceptors in OPVs.

4. Experimental sections

4.1 Materials

ECA and IN were purchased from TCI. Piperidine, triethylamine, chloroform and *tert*-butanol were purchased from Aldrich. All chemicals were used without further purification, and all reactions were performed under nitrogen atmosphere with anhydrous solvents.

4.2 Physical measurements

NMR spectra were recorded on a Bruker AVANCE II 400 spectrometer and elemental analyses were performed with a Flash EA 1112 series from Thermo Electron Corporation. TGA and DSC were performed on a TGA/DSC 1 thermogravimetric analyzer from Mettler-Toledo Inc. TGA was performed under a nitrogen atmosphere at a heating rate of 10 °C/min and DSC was performed at the heating and cooling rates of 10 °C/min under a nitrogen atmosphere. UV-vis spectra were obtained using a Shimadzu UV-2550 spectrometer and the films were prepared by spin coating from *o*-DCB solution. The E_g^{opt} were estimated from the absorption onset wavelengths (E_g^{opt} = 1240/λ_{onset} (eV)) of the films. The electrochemical properties of the small molecules were studied by CV measurement with a BAS 100B electrochemical analyzer. A three-electrode system was used and consisted of a non-aqueous reference electrode (0.1 M Ag/Ag^+ acetonitrile solution), a platinum working electrode, and a platinum wire as the counter electrode. The oxidation and reduction potentials of the small molecules were measured in acetonitrile with 0.1 M (n-$C_4H_9)_4N$-PF_6. The films were prepared by dip-coating from a solution of the small molecules onto the platinum working electrode, and the measurements were calibrated using the ferrocene value –4.8 eV as the standard. The AFM images were obtained with the Digital Instruments Nanoscope IV. The AFM measurements were performed on the same samples that were used as the top layer in the OPV devices (ITO/PEDOT:PSS/P3HT:acceptor).

4.3 Fabrication of OPVs devices

PEDOT:PSS (Clevios P VP AI 4083) was purchased from Heraeus. The OPV cells were fabricated with the configuration ITO/PEDOT:PSS/P3HT:acceptor/LiF/Al. The ITO glass was cleaned with sequential ultrasonic treatment in detergent, deionized water, acetone, and isopropyl alcohol for 15 min and subsequently dried in an oven for 5 h. They were then pre-treated in a UV-ozone oven for 15 min and spin-coated with a layer of PEDOT:PSS (~30 nm). Subsequently, the BHJ active layer was spin-cast at 3000 rpm from a D/A solution in *o*-DCB with a total solids concentration of 40 mg mL^{-1}. The average thickness of the active layers (~200 nm) was measured with an Alpha-Step IQ surface profiler. A LiF (~0.5 nm) and Al (~100 nm) layer were directly deposited onto the active layer under a vacuum of ~10^{-6} Torr. The effective area of all devices was measured to be 9 mm^2. The *J-V* curves of the devices were measured using a computer-controlled Keithley 236 source measure unit. Characterization of the un-encapsulated solar cells was carried out in air under AM 1.5G illumination, 100 mW cm^{-2}, using a xenon lamp-based solar simulator. The simulator irradiance was characterized using a calibrated spectrometer, and the illumination intensity was set using an NREL-certified silicon diode with an integrated KG1 optical filter. The EQE was measured using a reflective microscope objective to focus the light output from a 100 W halogen lamp outfitted with a monochromator and optical chopper (PV Measurements, Inc.). The photocurrent was measured using a lock-in amplifier, and the absolute photon flux was determined using a calibrated silicon photodiode.

4.4 Hole and electron mobility measurements

Hole-only and electron-only devices were fabricated with the structures of ITO/PEDOT:PSS/P3HT:small molecule/Au and ITO/ZnO/P3HT:small molecule/Ca/Al, respectively. The hole and electron mobility of the P3HT:small molecule films were measured by using the SCLC method by using the following equation:[31]

$$J = \frac{9}{8}\varepsilon_0\varepsilon_r\mu\frac{V^2}{L^3}$$

In the equation, J is the current density, ε_0 is the permittivity of free space, ε_r is the dielectric constant of the materials, μ is the charge carrier mobility, L is the thickness of the active layer and V is the voltage drop across the device. The *J-V* curves of the devices were recorded on a computer-controlled Keithley 236 source measure unit.

4.5 Synthesis of small molecules

5,5'-(N-9''-heptadecanylcarbazole-2,7-diyl)bis(thiophene-2-carbaldehyde) (Cz-T-CHO), 5,5'-(9,9-dioctyl-9H-fluorene-2,7-diyl)bis(thiophene-2-carbaldehyde) (Flu-T-CHO), **Cz-RH** and **Flu-RH** were synthesized according to the literature.[21-22]

Cz-ECA. Cz-T-CHO (0.30 g, 0.48 mmol) was dissolved in a solution of dry chloroform (50 mL), and three drops of triethylamine followed by ECA (1.3 g, 11.5 mmol) were added. The resulting solution was stirred for 3 days at room temperature. The reaction mixture was then extracted with dichloromethane and water. The collected organic layer was dried over $MgSO_4$. After removing the solvent under reduced pressure, the crude product was purified by silica gel chromatography using a mixture of dichloromethane and petroleum ether (3:1) as an eluent and then recrystallized from dichloromethane and ethanol to give the product as a red powder (0.28 g, yield 72%). ^{1}H NMR ($CDCl_3$, 400MHz): δ (ppm) 8.23 (s, 2H), 8.13 (m, 2H), 7.65-7.86 (m, 4H), 7.60 (d, J = 8.3 Hz, 2H), 7.53 (m, 2H), 4.65 (m, 1H), 4.40 (m, 4H), 2.32 (m, 2H), 2.02 (m, 2H), 1.43 (m, 6H), 1.01-1.25 (m, 24H), 0.78 (t, J = 6.9 Hz, 6H) (The multiple proton peaks are due to atropisomerism).[32] ^{13}C NMR ($CDCl_3$, 100MHz): δ (ppm) 163.06, 155.97, 155.86, 146.57, 146.41, 143.20, 139.84, 139.34, 138.94, 134.86, 130.96, 130.51, 124.57, 123.23,

121.48, 121.21, 118.40, 118.17, 116.14, 109.31, 106.86, 97.79, 97.65, 62.49, 56.90, 33.86, 31.73, 29.38, 29.27, 29.14, 26.71, 22.58, 14.27, 14.04 (The multiple carbon peaks are due to atropisomerism).[32] Anal. Calcd for $C_{49}H_{57}N_3O_4S_2$: C, 72.11; H, 7.04; N, 5.15; O, 7.84; S, 7.86. Found: C, 71.63; H, 7.31; N, 5.25; S, 7.55.

Flu-ECA. This compound was prepared in the same manner as **Cz-ECA** using Flu-T-CHO (0.30 g, 0.48 mmol) and ECA (1.3 g, 11.5 mmol) in chloroform (50 mL) to give a orange powder (0.26 g, 67%). ^{1}H NMR ($CDCl_3$, 400MHz): δ (ppm) 8.35 (s, 2H), 7.78 (m, 6H), 7.66 (m, 2H), 7.52 (m, 2H), 4.43 (m, 4H), 2.10 (m, 4H), 1.43 (m, 6H), 1.07-1.19 (m, 20H), 0.80 (t, *J* = 7.0 Hz, 6H), 0.65 (m, 4H). ^{13}C NMR ($CDCl_3$, 100MHz): δ (ppm) 163.03, 155.16, 152.38, 146.57, 141.85, 139.33, 134.83, 132.18, 125.89, 124.42, 120.87, 120.58, 116.13, 97.77, 62.51, 55.77, 40.21, 31.74, 29.83, 29.17, 29.16, 23.77, 22.58, 14.27, 14.05. Anal. Calcd for $C_{49}H_{56}N_2O_4S_2$: C, 73.46; H, 7.05; N, 3.50; O, 7.99; S, 8.01. Found: C, 73.77; H, 7.38; N, 3.57; S, 7.94.

Cz-IN. Three drops of piperidine were added to a solution of Cz-T-CHO (0.30 g, 0.48 mmol) and IN (0.21 g, 1.4 mmol) in *tert*-butanol (11 mL). The resulting solution was stirred under reflux for 24 h and cooled to 50 ℃. Ethanol (5 mL) was added and the reaction allowed to cool to room temperature. The precipitate was filtered off, washed with ethanol and recrystallized from dichloromethane/acetone (5 mL/20 mL) to give the product as a red solid (0.36 g, yield 86%). ^{1}H NMR ($CDCl_3$, 400MHz): δ (ppm) 8.18 (m, 2H), 8.12 (m, 1H), 7.98-8.06 (m, 8H), 7.83 (m, 5H), 7.73 (m, 2H), 7.63 (m, 2H), 4.73 (m, 1H), 2.40 (m, 2H), 2.08 (m, 2H), 1.07-1.31 (m, 24H), 0.79 (t, *J* = 6.8 Hz, 6H) (The multiple proton peaks are due to atropisomerism).[32] ^{13}C NMR ($CDCl_3$, 100MHz): δ (ppm) 190.35, 189.63, 158.61, 143.78, 143.67, 143.54, 143.22, 142.03, 140.47, 139.88, 136.71, 136.61, 136.13, 136.04, 134.96, 134.75, 131.43, 131.01, 124.98, 124.60, 123.82, 123.70, 123.26, 122.97, 122.77, 121.36, 121.11, 118.49, 118.24, 109.27, 106.84, 56.92, 33.94, 31.76, 29.48, 29.36, 29.21, 26.85, 22.60, 14.06 (The multiple carbon peaks are due to atropisomerism).[32] Anal. Calcd for $C_{57}H_{55}NO_4S_2$: C, 77.60; H, 6.28; N, 1.59; O, 7.25; S, 7.27. Found: C, 77.27; H, 6.04; N, 1.49; S, 6.22.

Flu-IN. This compound was prepared in the same manner as **Cz-IN** using Flu-T-CHO (0.30 g, 0.49 mmol) and IN (0.21 g, 1.4 mmol) in *tert*-butanol (11 mL) to give an orange powder (0.36 g, 86%). A sample for EA was recrystallised from toluene/petroleum ether. ^{1}H NMR ($CDCl_3$, 400MHz): δ (ppm) 8.00-8.05 (m, 8H), 7.80-7.87 (m, 8H), 7.78 (m, 2H), 7.60 (d, *J* = 4.1 Hz, 2H), 2.13 (m, 4H), 1.02-1.25 (m, 20H), 0.79 (t, *J* = 7.0 Hz, 6H), 0.68 (m, 4H). ^{13}C NMR ($CDCl_3$, 100MHz): δ (ppm) 190.38, 189.88, 157.91, 152.40, 143.78, 142.02, 141.92, 140.56, 136.63, 136.24, 135.06, 134.87, 132.72, 125.94, 124.88, 123.85, 123.05, 122.83, 120.82, 120.72, 55.80, 40.29, 31.76, 29.91, 29.22, 29.19, 23.83, 22.58, 14.04. Anal. Calcd for $C_{57}H_{54}O_4S_2$: C, 78.95; H, 6.28; O, 7.38; S, 7.40. Found: C, 78.27; H, 6.32; S, 7.83.

Acknowledgements

This work was supported by the National Research Foundation of Korea (NRF) Grant funded by the Korean Government (MSIP) (No. NRF-2015R1A1A3005083).

Notes and references

[a] Department of Chemistry, Kyonggi University, San 94-6, Iui-dong, Yeongtong-gu, Suwon-si, Gyeonggi 443-760, Republic of Korea. E-mail: ehlim@kyonggi.ac.kr
[b] Korea Research Institute of Chemical Technology (KRICT), 100 Jang-dong, Yuseong-gu, Daejeon 305-600, Republic of Korea.

† Electronic supplementary information (ESI) available: ^{1}H and ^{13}C NMR, additional photovoltaic properties under various conditions, and phase AFM images for the blend films. See DOI: 10.1039/x

1 (a) D. J. Burke and D. J. Lipomi, *Energ. Environ. Sci.*, 2013, **6**, 2053–2066; (b) F. C. Krebs and M. Jørgensen, *Sol. Energ. Mat. Sol. C.*, 2013, **119**, 73–76; (c) D. Konios, C. Petridis, G. Kakavelakis, M. Sygletou, K. Savva, E. Stratakis and E. Kymakis, *Adv. Funct. Mater*., 2015, **25**, 2213–2221; (d) T. P. Tyler, R. E. Brock, H. J. Karmel, T. J. Marks and M. C. Hersam, *Adv. Energ. Mater.*, 2011, **1**, 785–791; (e) M. M. Stylianakis, G. D. Spyropoulos, E. Stratakis and E. Kymakis, Carbon, 2012, **50**, 5554–5561; (f) E. Stratakis, K. Savva, D. Konios, C. Petridis and E. Kymakis, *Nanoscale*, 2014, **6**, 6925–6931; (g) G. Kakavelakis, D. Konios, E. Stratakis and E. Kymakis, *Chem. Mater.*, 2014, **26**, 5988–5993.

2 (a) A. Mishra and P. Bäuerle, *Angew. Chem. Int. Edit.*, 2012, **51**, 2020–2067; (b) J. J. M. Halls, C. A. Walsh, N. C. Greenham, E. A. Marseglia, R. H. Friend, S. C. Moratti and A. B. Holmes, *Nature*, 1995, **376**, 498–500; (c) G. Yu, J. Gao, J. C. Hummelen, F. Wudl and A. J. Heeger, *Science*, 1995, **270**, 1789–1791.

3 J. You, L. Dou, K. Yoshimura, T. Kato, K. Ohya, T. Moriarty, K. Emery, C.-C. Chen, J. Gao, G. Li and Y. Yang, *Nat. Commun.*, 2013, **4**, 1446.

4 Y. Liu, C.-C. Chen, Z. Hong, J. Gao, Y. Yang, H. Zhou, L. Dou and G. Li, *Sci. Rep.*, 2013, **3**, 3356.

5 (a) B. C. Thompson and J. M. J. Fréchet, *Angew. Chem. Int. Edit.*, 2007, **47**, 58–77; (b) L. Dou, J. You, Z; Hong, Z. Xu, G. Li, R. A. Street and Y. Yang, *Adv. Mater.*, 2013, **25**, 6642–6671; (c) D. Mi, J.-H. Kim, H. U. Kim, F. Xu and D.-H. Hwang, *J. Nanosci. Nanotechno.*, 2014, **14**, 1064–1084.

6 Y. He and Y. Li, *Phys. Chem. Chem. Phys.*, 2011, **13**, 1970–1983.

7 (a) A. a. F. Eftaiha, J.-P; Sun, I. G. Hill and G. C. Welch, *J. Mater. Chem. A*, 2014, **2**, 1201–1213; (b) P. Sonar, J. P. Fong Lim and K. L. Chan, *Energ. Environ. Sci.*, 2011, **4**, 1558–1574.

8 (a) H. U. Kim, J.-H. Kim, H. Suh, J. Kwak, D. Kim, A. C. Grimsdale, S.C. Yoon and D.-H. Hwang, *Chem. Commun.*, 2013, **49**, 10950–10952; (b) Y. Kim and E. Lim, *Polymers*, 2014, **6**, 382–407.

9 Z. Lu, B. Jiang, X. Zhang, A. Tang, L. Chen, C. Zhan and J. Yao, *Chem. Mater.*, 2014, **26**, 2907–2914.

10 X. Zhang, Z. Lu, L. Ye, C. Zhan, J. Hou, S. Zhang, B. Jiang, Y. Zhao, J. Huang, S. Zhang, Y. Liu, Q. Shi, Y. Liu and J. Yao, *Adv. Mater.*, 2013, **25**, 5791–5797.

11 Y. Zang, C.-Z. Li, C.-C. Chueh, S. T. Williams, W. Jiang, Z.-H. Wang, J.-S. Yu and A. K. Y. Jen, *Adv. Mater.*, 2014, **26**, 5708–5714.

12 (a) S.-L. Suraru and F. Würthner, *Angew. Chem. Int. Edit.*, 2014, **53**, 7428–7448; (b) G. Ren, E. Ahmed and S. A. Jenekhe, *Adv. Energy Mater.*, 2011, **1**, 946–953.

13 (a) J. T. Bloking, X. Han, A. T. Higgs, J. P. Kastrop, L. Pandey, J. E. Norton, C. Risko, C. E. Chen, J.-L. Brédas, M. D. McGehee and A. Sellinger, *Chem. Mater.*, 2011, **23**, 5484–5490; (b) Y. Fang, A. K.

Pandey, A. M. Nardes, N. Kopidakis, P. L. Burn and P. Meredith, *Adv. Energy Mater.*, 2013, **3**, 54–59.
14 A. Facchetti, *Mater. Today*, 2013, **16**, 123–132.
15 (a) J. Huang, X. Wang, X. Zhang, Z. Niu, Z. Lu, B. Jiang, Y. Sun, C. Zhan and J. Yao, *ACS Appl. Mater. Inter.*, 2014, **6**, 3853–3862; (b) A. Sharenko, C. M. Proctor, T. S. van der Poll, Z. B. Henson, T.-Q. Nguyen and G. C. Bazan, *Adv. Mater.*, 2013, **25**, 4403–4406; (c) P. Cheng, L. Ye, X. Zhao, J. Hou, Y. Li and X. Zhan, *Energ. Environ. Sci.*, 2014, **7**, 1351–1356.
16 Y. Liu, X. Wan, F. Wang, J. Zhou, G. Long, J. Tian, J. You, Y. Yang and Y. Chen, *Adv. Energy Mater.*, 2011, **1**, 771–775.
17 (a) W. Ni, M. Li, X. Wan, H. Feng, B. Kan, Y. Zuo and Y. Chen, *RSC Adv.*, 2014, **4**, 31977–31980; (b) J. Zhou, Y. Zuo, X. Wan, G. Long, Q. Zhang, W. Ni, Y. Liu, Z. Li, G. He, C. Li, B. Kan, M. Li and Y. Chen, *J. Am. Chem. Soc.*, 2013, **135**, 8484–8487; (c) N. Lim, N. Cho, S. Paek, C. Kim, J. K. Lee and J. Ko, *Chem. Mater.*, 2014, **26**, 2283–2288.
18 B. Kan, Q. Zhang, M. Li, X. Wan, W. Ni, G. Long, Y. Wang, X. Yang, H. Feng and Y. Chen, *J. Am. Chem. Soc.*, 2014, **136**, 15529–15532.
19 (a) S. Shen, P. Jiang, C. He, J. Zhang, P. Shen, Y. Zhang, Y. Yi, Z. Zhang, Z. Li and Y. Li, *Chem. Mater.*, 2013, **25**, 2274–2281; (b) W, Tang, D. Huang, C. He, Y. Yi, J. Zhang, C. Di, Z. Zhang and Y. Li, *Org. Electron.*, 2014, **15**, 1155–1165.
20 G. He, Z. Li, X. Wan, J. Zhou, G. Long, S. Zhang, M. Zhang and Y. Chen, *J. Mater. Chem. A*, 2013, **1**, 1801–1809.
21 Y. Kim, C. E. Song, S.-J. Moon and E. Lim, *Chem. Commun.*, 2014, **50**, 8235–8238.
22 K. N. Winzenberg, P. Kemppinen, F. H. Scholes, G. E. Collis, Y. Shu, T. Birendra Singh, A. Bilic, C. M. Forsyth and S. E. Watkins, *Chem. Commun.*, 2013, **49**, 6307–6309.
23 S. Holliday, R. Ashraf, C. Nielsen, M. Kirkus, J. Rohr, C.-H. Tan, E. Collado-Fregoso, A.-C. Knall, J. Durrant, J. Nelson and I. McCulloch, *J. Am. Chem. Soc.*, 2015, **137**, 898–904.
24 (a) O. Kwon, J. Jo, B. Walker, G. C. Bazan and J. H. Seo, *J. Mater. Chem.*, 2013, **1**, 7118–7124; (b) C. E. Song, I.-N. Kang, J.-H. Kim, D.-H. Hwang, J.-C. Lee, T. Ahn, W. S. Shin, S.-J. Moon and S. K. Lee, *J. Poly. Sci. Part A: Pol. Chem.* 2013, **51**, 1512–1519.
25 (a) M. C. Scharber, D. Mühlbacher, M. Koppe, P. Denk, C. Waldauf, A. J. Heeger and C. J. Brabec, *Adv. Mater.*, 2006, **18**, 789–794; (b) T. Ameri, P. Khoram, J. Min and C. J. Brabec, *Adv. Mater.*, 2013, **25**, 4245–4266.
26 T. V. Pho, F. M. Toma, B. J. Tremolet de Villers, S. Wang, N. D. Treat, N. D. Eisenmenger, G. M. Su, R. C. Coffin, J. D. Douglas, J. M. J. Fréchet, G. C. Bazan, F. Wudl and M. L. Chabinyc, *Adv. Energy Mater.*, 2014, **4**, 1301007.
27 Y.-J. Cheng, S.-H. Yang and C.-S. Hsu, *Chem. Rev.*, 2009, **109**, 5868–5923.
28 P. P. Khlyabich, B. Burkhart and B. C. Thompson, *J. Am. Chem. Soc.*, 2011, **133**, 14534–14537.
29 R. Zhang, B. Li, M. C. Iovu, M. Jeffries-El, G. Sauvé, J. Cooper, S. Jia, S. Tristram-Nagle, D. M. Smilgies, D. N. Lambeth, R. D. McCullough and T. Kowalewski, *J. Am. Chem. Soc.*, 2006, **128**, 3480–3481.
30 (a) A. Opitz, J. Wagner, W. Brütting, A. Hinderhofer and F. Schreiber, *Phys. Status Solidi A*, 2009, **206**, 2683–2694; J. A. Kong, E. Lim, K. K. Lee, S. Lee and H. S. Kim, *Sol. Energ. Mat. Sol. C.*, 2010, **94**, 2057–2063.
31 L. Dou, J. You, J. Yang, C.-C. Chen, Y. He, S. Murase, T. Moriarty, K. Emery, G. Li and Y. Yang, *Nat. Photon.*, 2012, **6**, 180–185.
32 (a) I. Grosu, G. Plé, S. Mager, E. Mesaros, A. Dulau and C. Gego, *Tetrahedron*, 1998, **54**, 2905–2916; (b) A. N. Cammidge and K. V. L. Crépy, *J. Org. Chem.*, 2003, **68**, 6832–6835; (c) J. Clayden, *Tetrahedron*, 2004, **60**, 4335.

Table of Contents

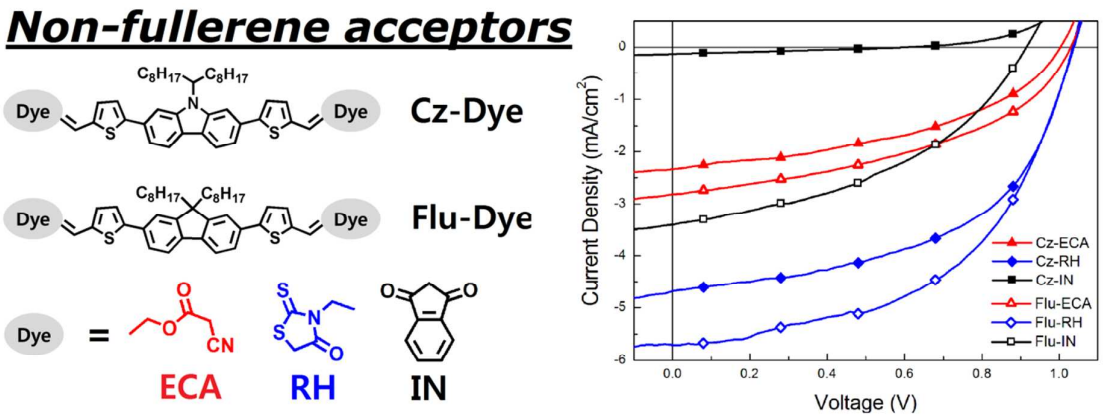

Fluorene- and carbazole-based small molecules with dye end groups were synthesized for use as non-fullerene acceptors in organic photovoltaic cells.